PHYSICAL REVIEW APPLIED **13,** 011002 (2020)

Letter

Plasmonic Gas Sensing with Graphene Nanoribbons

Kaveh Khaliji,[1,*] Sudipta Romen Biswas,[1] Hai Hu,[2,3] Xiaoxia Yang,[2,3] Qing Dai,[2,3]
Sang-Hyun Oh,[1] Phaedon Avouris,[4] and Tony Low[1,†]

[1] *Department of Electrical and Computer Engineering, University of Minnesota, Minneapolis, Minnesota 55455, USA*
[2] *Division of Nanophotonics, CAS Center for Excellence in Nanoscience, National Center for Nanoscience and Technology, Beijing 100190, P. R. China*
[3] *University of Chinese Academy of Sciences, Beijing 100049, P. R. China*
[4] *IBM T. J. Watson Research Center, Yorktown Heights, New York 10598, USA*

(Received 13 July 2019; revised manuscript received 24 September 2019; published 22 January 2020)

The main challenge to exploiting plasmons for gas vibrational mode sensing is the extremely weak infrared absorption of gas species. In this work, we explore the possibility of trapping free-gas molecules via surface adsorption, optical, or electrostatic fields to enhance gas-plasmon interactions and to increase plasmon-sensing ability. We discuss the relative strengths of these trapping forces and find gas adsorption in a typical nanoribbon array plasmonic setup produces measurable dips in optical extinction of magnitude 0.1% for a gas concentration of about the parts per thousand level.

DOI: 10.1103/PhysRevApplied.13.011002

Introduction. Two-dimensional (2D) materials have garnered considerable attention as a platform for gas sensing, owing to their large surface-to-volume ratio, which renders their electronic properties very sensitive to environmental influences, such as adsorbed molecules or external field [1–3]. Thus far, gas sensing based on extended 2D materials has relied on schemes involving changes in conductance [4–6], surface work function [7,8], or their contact-barrier heights [9,10], with the main underlying mechanism being charge redistribution due to physical or chemical adsorption. These sensors function at room temperature, require relatively low input power, and can be highly sensitive. Their major drawback is poor gas specificity, due to the lack of spectroscopic identification of a particular species, so they cannot differentiate between various analytes within a gas mixture.

Plasmon-enhanced infrared optical absorption based on 2D materials is regarded to be a promising spectroscopic technique for probing vibrational modes of large complex biopolymers (proteins, nucleic acids, synthetic polymers, or adsorbed molecular layers), as it enables high-fidelity mode sensing at room temperature [11–16]. To be able to excite the 2D plasmon by direct optical excitation, nanoribbon arrays have been used [17,18]. This technique, however, has not been proven to be as effective in identifying the vibrational modes of gas molecules, where the main challenge is the small absorption strength of the vibrational modes of individual molecules compared to biopolymers. However, the gas dielectric response is proportional to its concentration. This suggests via trapping molecules close to 2D material, one might be able to enhance the interaction of gas molecules with the evanescent plasmon fields. In fact, a recent work has shown that a significant increase in gas density atop graphene would be needed for selective gas detection via graphene plasmons [19]. Here, we verify what physical mechanism can provide sufficient trapping for gas identification with graphene plasmons.

In a plasmon-based sensing setup, the analyte species may interact with the incident optical field [20–22], sensing material surface (via adsorption) [23,24], and the applied bias field [25–28]. These interactions have also been exploited in 2D-based platforms to control the positioning of nanoparticles [29–33]. In this work, we calculate the contributions of each of the three mechanisms (optical field, bias electrostatic field, and adsorption) in redistributing a homogeneous gas and thus facilitating gas sensing via plasmon excitation in a graphene nanoribbon (GNR) array sensor geometry.

Trapping Molecules. The sensor geometry is illustrated in Fig. 1(a), where a simple metal-oxide GNR is used to tune electrostatic doping in graphene. The gas is in direct contact with the GNR array. The incident light is impinging normally on the device with polarizations parallel and perpendicular to the GNR array. The reflected light is spectrally analyzed for gas signatures. The gas dielectric function is assumed to follow a Lorentzian form

---

[*] khali161@umn.edu
[†] tlow@umn.edu

with frequency, ω, within the spectral window of interest [34,35]:

$$\epsilon_g = 1 + \frac{\Delta\epsilon\Omega^2}{\Omega^2 - \omega^2 - i\gamma\omega}, \qquad (1)$$

where one IR-active vibrational mode is considered for the gas; the mode is characterized by its frequency Ω, linewidth γ, and absorption weight $\Delta\epsilon$. We use $\Omega = 1300\ \mathrm{cm}^{-1}$ and $\gamma = 10\ \mathrm{cm}^{-1}$ as representative gas parameters. The absorption weight varies linearly with the gas concentration, i.e. $\Delta\epsilon = p_0\mathcal{C}$ [19,36], with the proportionality constant $p_0 = 10\ \mathrm{cm}^3/\mathrm{mol}$ [19]. The dielectric function in Eq. (1) is used for gas in both free and trapped states. The polarizability of the gas can then be obtained via [37]:

$$\alpha_g = \frac{3\epsilon_0}{\mathcal{C}}\left(\frac{\epsilon_g - 1}{\epsilon_g + 2}\right), \qquad (2)$$

where ϵ_0 is the vacuum permittivity. The gas dielectric function at 1 and 10 parts per thousand (ppt) are shown in Fig. 1(b). Accordingly, the gas dielectric function can be tuned through its concentration, the peak magnitudes in both real and imaginary parts of ϵ_g vary linearly with concentration.

For gas molecules treated as classical particles in thermal equilibrium, the connection between local gas concentration, $\mathcal{C}(x,z)$ and trapping potential, $\mathcal{U}(x,z)$ can be obtained via statistical arguments [38,39]:

$$\mathcal{C} = \frac{hl\mathcal{C}_t\left[1 + \exp\left(-\beta\mathcal{U}\right)\Theta\left(-1 - \beta\mathcal{U}\right)\right]}{hl + \int_{-\beta\mathcal{U}\geqslant 1}\exp\left(-\beta\mathcal{U}\right)\,dx\,dz}, \qquad (3)$$

where $\Theta(\cdot)$ is the step function, h is the height of the gas chamber, and l is the array period [see Fig. 1(a)]. We consider $W = 50$ nm and $f = 0.7$ for the GNR width and width-to-period ratio, respectively. We note the setup has translational symmetry along the y coordinate, and hence trapping potentials do not depend on y. The initial gas distribution is uniform with the concentration $\mathcal{C}_t$; unless denoted otherwise, 10 ppt is taken for its value.

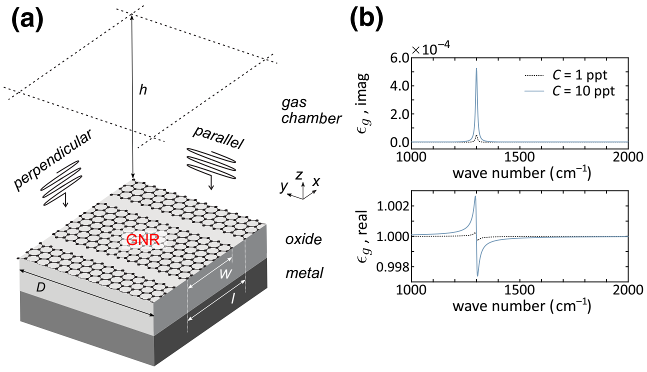

FIG. 1. (a) Schematic of the sensor setup. (b) Real and imaginary parts of gas permittivity versus wave number for 1 and 10 ppt gas concentrations under standard temperature-pressure condition.

The last input is the trapping potential, to be written as a sum of two terms, one repulsive and the other attractive. The former is dominant when the molecule is in close vicinity to the surface and is modeled as an infinite potential for $z < z_0$ [40], with z_0 the equilibrium distance between the adsorbed molecule and graphene, and is comparable with molecule radius. The attractive term depends on the trapping mechanism involved and is to be developed for each mechanism separately. For adsorption, this is approximated via

$$\mathcal{U}_{\mathrm{ad}} = -D_0\exp\left[-\gamma_0(z - z_0)\right], \quad |x| < W/2, \qquad (4)$$

which coincides in form with the attractive term in Morse potential commonly used to describe van der Waals interaction [41,42]. D_0 denotes the binding energy of the molecule-2D material system, and γ_0 is related to the potential force constant close to z_0. Here, we assume $\gamma_0 = 10\ \mathrm{nm}^{-1}$, $D_0 = 0.3$ eV, and $z_0 = 0.3$ nm [43–45].

To determine the effect of the electrostatic gate bias, we solve for a self-consistent solution of Poisson's equation and the graphene net electron density [33]:

$$\begin{gathered}\vec{\nabla}.\left(\epsilon\vec{\nabla}\phi\right) = en(x)\delta(z)/\epsilon_0,\\ n(x) = \frac{1}{\pi}\left[\frac{\mu(x)}{\hbar v_F}\right]^2 - n_D, \quad |x| < W/2,\end{gathered} \qquad (5)$$

where e is the electron charge, $\phi(x,z)$ is the electrostatic potential, $v_F = 10^8\ \mathrm{cm\,s}^{-1}$ is the graphene Fermi velocity. ϵ is the spatially varying dielectric constant, which is assumed to be unity within the chamber and is equal to $\epsilon_{\mathrm{ox}} = 2.5$ for the oxide region. $\mu(x)$ is the position-dependent chemical potential, which is given by $\mu(x) = e\phi(x, z = 0)$. n_D is the density of donor impurities in chemically doped graphene and is set to be $1.45 \times 10^{13}\ \mathrm{cm}^{-2}$. The problem is solved with COMSOL Multiphysics, AC/DC Module, where we applied the Dirichlet, periodic, and Neumann boundary conditions for the bottom, sides, and top edges of the simulation domain, respectively. The electrostatic force acting on a molecule is computed via $\vec{F}_{\mathrm{es}} = \frac{1}{2}\alpha_0\vec{\nabla}|\vec{E}|^2$ and the potential energy due to induced dipole is given by $\mathcal{U}_{\mathrm{es}} = -\int\vec{F}_{\mathrm{es}}\cdot d\vec{r}$, where $\alpha_0 = 10^{-36}\ \mathrm{F\,cm}^2$ is the static polarizability of a typical gas molecule [46,47].

The optical force is calculated using $\vec{F}_{\mathrm{op}} = \frac{1}{4}\Re\{\alpha_g\}\vec{\nabla}|\vec{E}|^2$, where $\vec{E}$ is the sum of incident and reflected fields at a given point [20,48]. Force calculations are performed using COMSOL Multiphysics, rf module, and the corresponding potential energy is computed with $\mathcal{U}_{\mathrm{op}} =$

$-\int \vec{F}_{\mathrm{op}} \cdot d\vec{r}$, implying that the optical potential energy is governed by the light intensity at a given point in the chamber.

With the numerical recipes at our disposal, we proceed with the discussion of these trapping potentials and their relative abilities in trapping the free gas. We begin with the optical force and its potential energy, as summarized in Fig. 2. The ribbon edges constitute the hotspots for optical trapping. This is expected as the underlying plasmon field decays quickly away from the edges [39,49]. Our simulations show the depth of the trapping potential increases linearly with the intensity of the incident light. Despite this trend, however, for power intensities typically used in FTIR experiments (0.01–50 $\mathrm{kW/cm^2}$), the maximum depth of the trapping potential is much smaller than the thermal energy at room temperature. Thus, for the geometry shown in Fig. 1(a), the field enhancement due to plasmon excitation does not help in trapping the molecules for sensing. We should point out, however, that the conclusion drawn here is for gas molecules atop graphene under plane-wave illumination. The optical trapping force can be enhanced for molecules with larger $\Delta\epsilon$ under tightly focused light fields [50], or for other 2D systems, which exhibit in-plane hyperbolic response with larger plasmon-induced field confinement close to the material surface [51].

We next look into electrostatic potential due to gate bias. From Fig. 3(a), the trapping hotspots again reside at the ribbon edges, and the potential energy decreases in magnitude rapidly towards the center, which is qualitatively similar to what we observed for the optical force. From Fig. 3(b), with increasing bias or reducing oxide thickness, the region where the electrostatic potential can surpass thermal energy becomes wider. For the assumed z_0 and with the repulsive potential included, 20-V bias across 5-nm-thick oxide are needed for the electrostatic potential to initiate gas trapping.

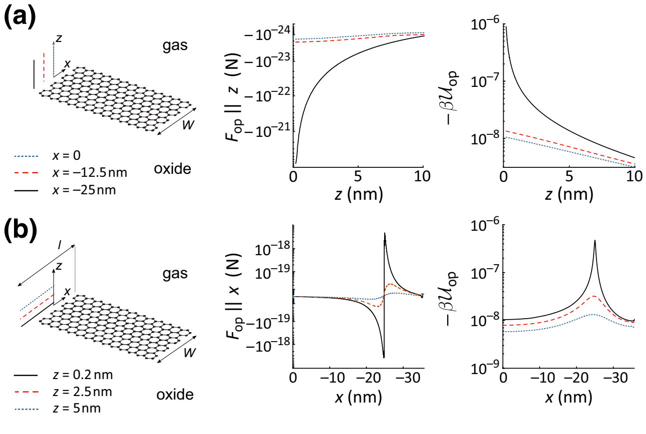

FIG. 2. (a) z-component of optical force and optical potential energy along the cutlines parallel to the z axis, with $x = 0$, -12.5, and -25 nm. (b) x-component of optical force and optical potential energy along the cutlines parallel to the x axis, placed 0.2, 2.5, and 5 nm above graphene. The data are computed at 1295 $\mathrm{cm^{-1}}$ with 0.05 $\mathrm{kW/cm^2}$ as input power density.

Lastly, we focus on surface adsorption and its effect on redistributing the gas molecules. In Fig. 4(a) the adsorption potential and the corresponding concentration of trapped molecules versus vertical distance from the graphene surface are depicted. The inset shows the linear dependence of the surface density of adsorbed molecules, n_{ad} as a function of the concentration of free molecules in the chamber. The slope increases for a larger binding energy, which could occur in defective graphene, or via introducing chemical dopants [44,52,53]. Our calculations show that for 5-nm oxide thickness, 20-V bias, and z_0 as small as 0.1 nm, the maximum trapped concentration due to adsorption remains larger (roughly 10^4) compared to that of the electrostatic trapping, which indicates that adsorption is the main mechanism that redistributes the free gas.

Plasmon-Based Sensing. For gas modes to appear vividly in the sensor response one needs for the graphene plasmon resonance to match the gas characteristic mode while the quarter-wavelength condition is also satisfied.

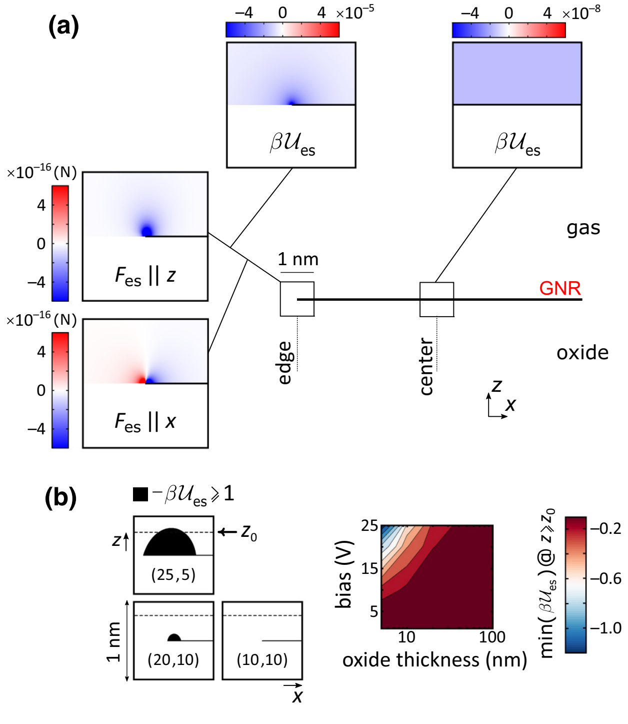

FIG. 3. (a) Spatial profile for electrostatic force components and potential energy in 1-nm vicinity of the ribbon edges. The potential energy at the ribbon center is also shown. The results are obtained for 10-V bias and oxide thickness of 1.22 μm. (b) Left: the region where the attractive electrostatic energy is smaller in magnitude relative to thermal energy. Data are shown for three pairs of (bias V, thickness nm). Right: the minimum electrostatic potential energy for $z \geq z_0$ as functions of bias and oxide thickness.

These criteria restrict both the oxide choice and oxide thickness ($\epsilon_{\text{ox}} \leq 5$ and thickness of 0.5 μm or more are needed), for typical background dopings ($n_D \lesssim 5 \times 10^{13}$ cm^{-2}) in graphene [54]. We, therefore, focus in this section on how adsorption may facilitate gas sensing with graphene plasmons. We define the plasmon extinction as 1-$R^g_{\text{per}}/R^g_{\text{par}}$, where R^g_{per} and R^g_{par} are the reflected powers when the chamber is filled with gas and the incident light is polarized along the x and y axes, respectively (for an alternative extinction definition see Ref. [39]). The adsorption affects the sensor response through: (i) gas redistribution, which is incorporated via Eqs. (1) and (3) with the adsorption potential as input, we define accordingly an effective conductivity for the adsorbed layer: $\sigma_{\text{ad}} = -i\omega\epsilon_0 h_{\text{ad}}\left[\epsilon_g(n_{\text{ad}}/h_{\text{ad}}) - 1\right]$ [19], where h_{ad} denotes the height of the trapping region for which $-\beta\mathcal{U}_{\text{ad}} \geqslant 1$; (ii) doping through adsorption charge transfer. The latter is accounted for within the expression used for graphene conductivity [55]: $\sigma_{\text{gr}} = ie^2 v_F\sqrt{(n_D + n_{\text{ad}}Q)/\pi}/(\hbar\omega + i\eta)$, where $\eta = 50$ meV is the broadening and Q is the effective fractional charge transferred between graphene and one adsorbed molecule. For molecules that act as acceptors (donors) upon adsorption, Q is negative (positive); in this work $Q = -0.05$ is assumed [56].

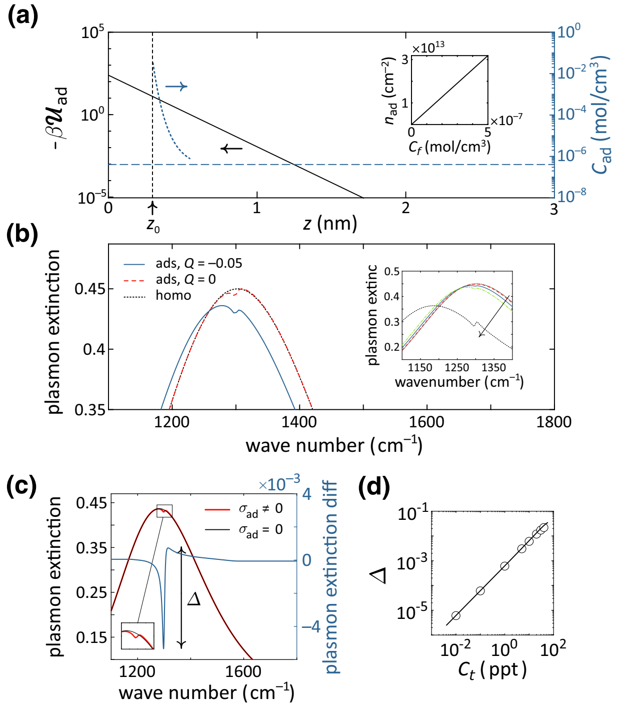

FIG. 4. (a) Adsorption potential and trapped gas concentration versus z. The horizontal dashed line denotes the $\mathcal{C}_t$. The inset shows the adsorbed surface density versus free-gas concentration. (b) Plasmon extinction for homogeneous and adsorbed gas (with and without adsorption charge transfer). The inset shows the plasmon extinction at various initial homogeneous gas concentration. Following the arrow $\mathcal{C}_t$ increases from 0.1, to 1, 5, 10, and 50 ppt. (c) Plasmon extinctions for σ_{ad} included and when it is set to zero. The corresponding plasmon-extinction difference is also shown. (d) Variation amplitude in plasmon-extinction difference versus gas homogeneous concentration. The solid line is obtained from the analytical model.

To examine how adsorption modifies plasmon extinction, we begin with a comparison between the homogeneous and adsorbed gas distributions in Fig. 4(b). For graphene plasmon, adsorption in principle may shift the resonance either via doping or through modifying the dielectric function atop graphene. The latter, however, is relatively weak for all relevant adsorption densities. This is shown in Fig. 4(b) where the extinction peaks for homogeneous gas distribution and adsorbed gas with $Q = 0$ (i.e., excluding adsorption charge transfer) are compared. Adsorption can affect the vibrational mode absorption strength in two ways, by tuning the gas concentration close to graphene (thereby modifying the mode weight) or by plasmon-gas mode resonance detuning. From the inset, it is clear that increasing the adsorbed density (via increasing $\mathcal{C}_t$ or D_0), results in more apparent gas-induced dips in the extinction. The inset data also imply that the mode weight is a more critical factor than detuning to control the amplitude of the dips in this setup.

We note that label-free plasmonic gas-sensing schemes, commonly rely on direct chemisorption or physisorption of gas molecules atop the plasmonic surface [19,57], with either wavelength shift or intensity inspection adopted as the sensing method [16,58]. The wavelength shift, however, is not generally gas specific, which restricts its use to situations in which sensing device is exposed to one gas only. In this work, the gas-graphene interaction involves physisorption. Moreover, we rely on intensity interrogation to achieve gas identification. In Fig. 4(c), the difference between plasmon extinctions when σ_{ad} is included and when it is set to zero, are shown. The zero case denotes the extinction when the plasmon shift triggered by adsorption charge transfer is included while the contribution due to adsorbed gas dielectric response (which is the origin of the extinction dips) is left out. The peak-to-peak variation in the extinction difference, denoted with Δ is then recorded as a function of gas concentration in Fig. 4(d). From this, we conclude that for gas concentration of ppt level, plasmon-extinction changes of the order 0.1% can be observed, a level measurable by common far-field spectroscopic techniques [19].

Finally, we note that a simple analytical model can be used to estimate the electromagnetic response of the sensor [59,60]. This is accomplished via introducing an equivalent conductivity for the total system of graphene ribbons and adsorbed molecules:

$$\underline{\boldsymbol{\sigma_t}}^{-1} = \frac{1}{f}\frac{1}{\sigma_{\text{gr}} + \sigma_{\text{ad}}}\underline{\mathbf{I}} + \begin{pmatrix} -\frac{1}{i\omega\mathcal{C}_c} & 0 \\ 0 & 0 \end{pmatrix}, \tag{6}$$

where, $\underline{\mathbf{I}}$ is the unity matrix and $\mathcal{C}_c = (l/\pi)\epsilon_0\left[\epsilon_{\text{ox}} + \epsilon_g\left(\mathcal{C}_t - n_{\text{ad}}/h\right)\right]\log\{[\pi(1-f)/2]\}$ is the coupling capacitance. The transfer matrix method outlined in Ref. [61], is used to obtain the reflection spectra for the layered structure. From Fig. 4(d), the simple model recovers the magnitude change in gas-induced dips with the gas concentration.

Concluding Remarks. We examine the plasmonic sensing of gas vibrational modes using the graphene nanoribbon scheme. The sensitivity of gas detection depends on the trapping forces exerted on the gas molecules and by the confinement of the plasmonic field. These in turn also depend on the device structure. Here, through systematic modeling of the likely gas-trapping mechanisms in experiments (optical forces, electrostatic forces, and adsorption), we find that surface adsorption is the dominant mechanism in trapping free-gas molecules atop graphene, which then enables plasmon-enhanced sensing of the gas vibrational modes. Further increases in sensitivity are expected by utilizing a perfect absorption scheme [62,63] or the recently described approach [64] of placing an underlayer metal in close proximity to graphene to exploit extreme plasmon confinement due to the excitation of acoustic plasmons.

Acknowledgments. This research is supported by grants from the U.S. National Science Foundation (ECCS 1809723 to T.L. and S.-H.O. and ECCS 1809240 to S.-H.O.). S.-H.O. also acknowledges support from Seagate through the MINT consortium at the University of Minnesota.

[1] S. Yang, C. Jiang, and S.-h. Wei, Gas sensing in 2D materials, Appl. Phys. Rev. **4**, 021304 (2017).

[2] X. Liu, T. Ma, N. Pinna, and J. Zhang, Two-Dimensional nanostructured materials for gas sensing, Adv. Funct. Mater. **27**, 1702168 (2017).

[3] T. Wang, D. Huang, Z. Yang, S. Xu, G. He, X. Li, N. Hu, G. Yin, D. He, and L. Zhang, A review on graphene-based gas/Vapor sensors with unique properties and potential applications, Nano Micro Lett. **8**, 95 (2016).

[4] F. Schedin, A. Geim, S. Morozov, E. Hill, P. Blake, M. Katsnelson, and K. Novoselov, Detection of individual gas molecules adsorbed on graphene, Nat. Mater. **6**, 652 (2007).

[5] B. Zhan, C. Li, J. Yang, G. Jenkins, W. Huang, and X. Dong, Graphene field-effect transistor and its application for electronic sensing, Small **10**, 4042 (2014).

[6] A. N. Abbas, B. Liu, L. Chen, Y. Ma, S. Cong, N. Aroonyadet, M. Köpf, T. Nilges, and C. Zhou, Black phosphorus gas sensors, ACS Nano **9**, 5618 (2015).

[7] M. W. Nomani, V. Shields, G. Tompa, N. Sbrockey, M. Spencer, R. Webb, and G. Koley, Correlated conductivity and work function changes in epitaxial graphene, Appl. Phys. Lett. **100**, 092113 (2012).

[8] M. Qazi and G. Koley, NO_2 detection using microcantilever based potentiometry, Sensors **8**, 7144 (2008).

[9] A. Singh, M. A. Uddin, T. Sudarshan, and G. Koley, Tunable reverse-biased graphene/silicon heterojunction Schottky diode sensor, Small **10**, 1555 (2014).

[10] B. Liu, L. Chen, G. Liu, A. N. Abbas, M. Fathi, and C. Zhou, High-performance chemical sensing using Schottky-contacted chemical vapor deposition grown monolayer MoS_2 transistors, ACS Nano **8**, 5304 (2014).

[11] P. Avouris, T. F. Heinz, and T. Low, *2D Materials: Properties and Devices* (Cambridge University Press, Cambridge, 2017).

[12] X. Yang, Z. Sun, T. Low, H. Hu, X. Guo, F. J. García de Abajo, P. Avouris, and Q. Dai, Nanomaterial-based plasmon-enhanced infrared spectroscopy, Adv. Mater. **30**, 1704896 (2018).

[13] Y. Li, H. Yan, D. B. Farmer, X. Meng, W. Zhu, R. M. Osgood, T. F. Heinz, and P. Avouris, Graphene plasmon enhanced vibrational sensing of surface-adsorbed layers, Nano Lett. **14**, 1573 (2014).

[14] D. Rodrigo, O. Limaj, D. Janner, D. Etezadi, F. J. García De Abajo, V. Pruneri, and H. Altug, Mid-infrared plasmonic biosensing with graphene, Science **349**, 165 (2015).

[15] H. Hu, X. Yang, F. Zhai, D. Hu, R. Liu, K. Liu, Z. Sun, and Q. Dai, Far-field nanoscale infrared spectroscopy of vibrational fingerprints of molecules with graphene plasmons, Nat. Commun. **7**, 12334 (2016).

[16] D. B. Farmer, P. Avouris, Y. Li, T. F. Heinz, and S.-J. Han, Ultrasensitive plasmonic detection of molecules with graphene, ACS Photonics **3**, 553 (2016).

[17] L. Ju, B. Geng, J. Horng, C. Girit, M. Martin, Z. Hao, H. A. Bechtel, X. Liang, A. Zettl, Y. R. Shen, and F. Wang, Graphene plasmonics for tunable terahertz metamaterials, Nat. Nanotechnol. **6**, 630 (2011).

[18] H. Yan, T. Low, W. Zhu, Y. Wu, M. Freitag, Xuesong Li, F. Guinea, P. Avouris, and F. Xia, Damping pathways of mid-infrared plasmons in graphene nanostructures, Nat. Photonics **7**, 394 (2013).

[19] H. Hu, X. Yang, X. Guo, K. Khaliji, S. R. Biswas, F. J. García de Abajo, T. Low, Z. Sun, and Q. Dai, Gas identification with graphene plasmons, Nat. Commun. **10**, 1131 (2019).

[20] A. Jonáš and P. Zemánek, Light at work: The use of optical forces for particle manipulation, sorting, and analysis, Electrophoresis **29**, 4813 (2008).

[21] Y. Yuan, Y. Lin, B. Gu, N. Panwar, S. C. Tjin, J. Song, J. Qu, and K.-T. Yong, Optical trapping-assisted SERS platform for chemical and biosensing applications: Design perspectives, Coord. Chem. Rev. **339**, 138 (2017).

[22] W. Zhang, L. Huang, C. Santschi, and O. J. Martin, Trapping and sensing 10 nm metal nanoparticles using plasmonic dipole antennas, Nano Lett. **10**, 1006 (2010).

[23] K. Kurihara and K. Suzuki, Theoretical understanding of an absorption-based surface plasmon resonance sensor based on Kretchmann's theory, Anal. Chem. **74**, 696 (2002).

[24] T. Allsop, R. Arif, R. Neal, K. Kalli, V. Kundrát, A. Rozhin, P. Culverhouse, and D. J. Webb, Photonic gas sensors exploiting directly the optical properties of hybrid carbon nanotube localized surface plasmon structures, Light: Sci. Appl. **5**, e16036 (2016).

[25] A. Barik, L. M. Otto, D. Yoo, J. Jose, T. W. Johnson, and S.-H. Oh, Dielectrophoresis-enhanced plasmonic sensing with gold nanohole arrays, Nano Lett. **14**, 2006 (2014).

[26] S.-H. Oh, C. Escobedo, and A. G. Brolo, *Miniature Fluidic Devices for Rapid Biological Detection* (Springer, 2018).

[27] C. Schäfer, D. P. Kern, and M. Fleischer, Capturing molecules with plasmonic nanotips in microfluidic channels by dielectrophoresis, Lab Chip **15**, 1066 (2015).

[28] P. R. Gascoyne and J. Vykoukal, Particle separation by dielectrophoresis, Electrophoresis **23**, 1973 (2002).

[29] M. Engel, D. B. Farmer, J. T. Azpiroz, J.-W. T. Seo, J. Kang, P. Avouris, M. C. Hersam, R. Krupke, and M. Steiner, Graphene-enabled and directed nanomaterial placement from solution for large-scale device integration, Nat. Commun. **9**, 4095 (2018).

[30] J. Zhang, W. Liu, Z. Zhu, X. Yuan, and S. Qin, Towards nano-optical tweezers with graphene plasmons: Numerical investigation of trapping 10-nm particles with mid-infrared light, Sci. Rep. **6**, 38086 (2016).

[31] A. Marini, I. Silveiro, and F. J. García de Abajo, Molecular sensing with tunable graphene plasmons, ACS Photonics **2**, 876 (2015).

[32] B. Vasić and R. Gajić, Graphene-Covered Photonic Structures for Optical Chemical Sensing, Phys. Rev. Appl. **4**, 024007 (2015).

[33] A. Barik, Y. Zhang, R. Grassi, B. P. Nadappuram, J. B. Edel, T. Low, S. J. Koester, and S.-H. Oh, Graphene-edge dielectrophoretic tweezers for trapping of biomolecules, Nat. Commun. **8**, 1867 (2017).

[34] H. Haug and S. W. Koch, *Quantum Theory of the Optical and Electronic Properties of Semiconductors* (World Scientific Publishing Company, Singapore, 2009).

[35] S. G. Rodrigo, Terahertz gas sensor based on absorption-induced transparency, EPJ Appl. Metamater. **3**, 11 (2016).

[36] F. Liu and E. Cubukcu, Tunable omnidirectional strong light-matter interactions mediated by graphene surface plasmons, Phys. Rev. B **88**, 115439 (2013).

[37] D. J. Griffiths, *Introduction to Electrodynamics* (Pearson, San Francisco, 2008).

[38] C. Kittel and H. Kroemer, *Thermal Physics* (W. H. Freeman, New York, 1998).

[39] See Supplemental Material at http://link.aps.org/supplemental/10.1103/PhysRevApplied.13.011002 for the derivation of the spatially varying concentration, a comparison between optical field at the ribbon edge and center, and a discussion on device extinction.

[40] P. W. Atkins and J. De Paula, *Physical Chemistry* (Oxford University Press, Oxford UK, 1998).

[41] C. R. Weinberger and G. J. Tucker, *Multiscale Materials Modeling for Nanomechanics* (Springer, Cham, 2016).

[42] H. Pu, S. Rhim, M. Gajdardziksa-Josifovska, C. Hirschmugl, M. Weinert, and J. Chen, A statistical thermodynamics model for monolayer gas adsorption on graphene-based materials: Implications for gas sensing applications, RSC Adv. **4**, 47481 (2014).

[43] X.-Y. Liu, J.-M. Zhang, K.-W. Xu, and V. Ji, Improving SO_2 gas sensing properties of graphene by introducing dopant and defect: A first-principles study, Appl. Surf. Sci. **313**, 405 (2014).

[44] Y.-H. Zhang, Y.-B. Chen, K.-G. Zhou, C.-H. Liu, J. Zeng, H.-L. Zhang, and Y. Peng, Improving gas sensing properties of graphene by introducing dopants and defects: A first-principles study, Nanotechnology **20**, 185504 (2009).

[45] G. Lee, B. Lee, J. Kim, and K. Cho, Ozone adsorption on graphene: Ab initio study and experimental validation, J. Phys. Chem. C **113**, 14225 (2009).

[46] W. Duley and D. Williams, *Interstellar Chemistry* (Academic Press, New York, 1984).

[47] S. Sircar, Basic research needs for design of adsorptive gas separation processes, Ind. Eng. Chem. Res. **45**, 5435 (2006).

[48] L. Novotny and B. Hecht, *Principles of Nano-Optics* (Cambridge University Press, Cambridge, 2012).

[49] P. A. D. Gonçalves, E. J. C. Dias, Yu. V. Bludov, and N. M. R. Peres, Modeling the excitation of graphene plasmons in periodic grids of graphene ribbons: An analytical approach, Phys. Rev. B. **94**, 195421 (2016).

[50] N. Liu, M. L. Tang, M. Hentschel, H. Giessen, and A. P. Alivisatos, Nanoantenna-enhanced gas sensing in a single tailored nanofocus, Nat. Mater. **10**, 631 (2011).

[51] A. Nemilentsau, T. Low, and G. Hanson, Anisotropic Two-Dimensional Materials for Tunable Hyperbolic Plasmonics, Phys. Rev. Lett. **116**, 066804 (2016).

[52] J. Dai, J. Yuan, and P. Giannozzi, Gas adsorption on graphene doped with B, N, al, and S: A theoretical study, Appl. Phys. Lett. **95**, 232105 (2009).

[53] Y. Liu and J. Wilcox, CO_2 adsorption on carbon models of organic constituents of gas shale and coal, Environ. Sci. Technol. **45**, 809 (2010).

[54] H. Lee, K. Paeng, and I. S. Kim, A review of doping modulation in graphene, Synth. Met. **244**, 36 (2018).

[55] P. A. D. Gonçalves and N. M. Peres, *An Introduction to Graphene Plasmonics* (World Scientific, Singapore, 2016).

[56] L. Kong, A. Enders, T. S. Rahman, and P. A. Dowben, Molecular adsorption on graphene, J. Phys.: Condens. Matter **26**, 443001 (2014).

[57] T. Shegai, P. Johansson, C. Langhammer, and M. Käll, Directional scattering and hydrogen sensing by bimetallic Pd-Au nanoantennas, Nano Lett. **12**, 2464 (2012).

[58] A. Tittl, H. Giessen, and N. Liu, Plasmonic gas and chemical sensing, Nanophotonics **3**, 157 (2014).

[59] O. Kotov and Y. E. Lozovik, Enhanced optical activity in hyperbolic metasurfaces, Phys. Rev. B. **96**, 235403 (2017).

[60] K. Khaliji, A. Fallahi, L. Martin-Moreno, and T. Low, Tunable plasmon-enhanced birefringence in ribbon array of anisotropic two-dimensional materials, Phys. Rev. B. **95**, 201401 (2017).

[61] T. Zhan, X. Shi, Y. Dai, X. Liu, and J. Zi, Transfer matrix method for optics in graphene layers, J. Phys.: Condens. Matter **25**, 215301 (2013).

[62] S. Thongrattanasiri, F. H. Koppens, and F. J. G. De Abajo, Complete Optical Absorption in Periodically Patterned Graphene, Phys. Rev. Lett. **108**, 047401 (2012).

[63] S. Kim, M. S. Jang, V. W. Brar, K. W. Mauser, L. Kim, and H. A. Atwater, Electronically tunable perfect absorption in graphene, Nano Lett. **18**, 971 (2018).

[64] P. Alonso-González, A. Y. Nikitin, Y. Gao, A. Woessner, M. B. Lundeberg, A. Principi, N. Forcellini, W. Yan, S. Vélez, A. J. Huber *et al.*, Acoustic terahertz graphene plasmons revealed by photocurrent nanoscopy, Nat. Nanotechnol. **12**, 31 (2017).